Neurobiology of Aging 73 (2019) 171–176

Contents lists available at ScienceDirect

Neurobiology of Aging

journal homepage: www.elsevier.com/locate/neuaging

Comparison of longitudinal Aβ in nondemented elderly and Down syndrome

Dana L. Tudorascu [a,b], Stewart J. Anderson [b], Davneet S. Minhas [c], Zheming Yu [c], Diane Comer [a], Patrick Lao [d,e], Sigan Hartley [e,f], Charles M. Laymon [c,g], Beth E. Snitz [c], Brian J. Lopresti [c], Sterling Johnson [d,h], Julie C. Price [c,i], Chester A. Mathis [c], Howard J. Aizenstein [j], William E. Klunk [j], Benjamin L. Handen [j], Brad T. Christian [d,e], Ann D. Cohen [j,*]

[a] Department of Medicine, University of Pittsburgh, School of Medicine, Pittsburgh, PA, USA
[b] Department of Biostatistics, University of Pittsburgh, Graduate School of Public Health, Pittsburgh, PA, USA
[c] Department of Radiology, University of Pittsburgh School of Medicine, Pittsburgh, PA, USA
[d] Department of Medical Physics, University of Wisconsin, Madison School of Medicine, Madison, WI, USA
[e] Department of Waisman Center, University of Wisconsin, Madison School of Medicine, Madison, WI, USA
[f] Departments of Human Development and Family Studies, University of Wisconsin, Madison School of Medicine, Madison, WI, USA
[g] Department of Biongeenering, University of Pittsburgh, Pittsburgh, PA, USA
[h] Department of Medicine and Geriatrics, University of Wisconsin, Madison School of Medicine, Madison, WI, USA
[i] Massachusetts General Hospital, A. A. Martinos Center for Biomedical Imaging, Cambridge, MA, USA
[j] Department of Psychiatry, University of Pittsburgh, School of Medicine, Pittsburgh, PA, USA

ARTICLE INFO

Article history:
Received 18 July 2018
Received in revised form 21 September 2018
Accepted 23 September 2018
Available online 27 September 2018

Keywords:
Down syndrome
Amyloid
Alzheimer's disease

ABSTRACT

Down syndrome (DS) predisposes individuals to early Alzheimer's disease (AD). Using Pittsburgh Compound B ([^{11}C]PiB), a pattern of striatal amyloid beta (Aβ) that is elevated relative to neocortical binding has been reported, similar to that of nondemented autosomal dominant AD mutation carriers. However, it is not known whether changes in striatal and neocortical [^{11}C]PiB retention differ over time in a nondemented DS population when compared to changes in a nondemented elderly (NDE) population. The purpose of this work was to assess longitudinal changes in trajectories of Aβ in a nondemented DS compared to an NDE cohort. The regional trajectories for anterior ventral striatum (AVS), frontal cortex, and precuneus [^{11}C]PiB retention were explored over time using linear mixed effects models with fixed effects of time, cohort, and time-by-cohort interactions and subject as random effects. Significant differences between DS and NDE cohort trajectories for all 3 region of interests were observed ($p < 0.05$), with the DS cohort showing a faster accumulation in the AVS and slower accumulation in the frontal cortex and precuneus compared to the NDE cohort. These data add to the previously reported distinct pattern of early striatal deposition not commonly seen in sporadic AD by demonstrating that individuals with DS may also accumulate Aβ at a rate faster in the AVS when compared to NDE subjects.

1. Introduction

Definitive diagnosis of Alzheimer's disease (AD) relies on the demonstration of amyloid beta (Aβ) plaques and neurofibrillary tangles at autopsy (Hyman et al., 2012). The time course and cause of Aβ deposition in AD remains unclear but 2 main hypotheses are currently proposed: (1) impaired clearance, like that observed in later-life Aβ deposition seen in preclinical AD, mild cognitive impairment, and late-onset AD (Mawuenyega et al., 2010); and (2) altered processing or overproduction of amyloid precursor protein (APP), like that observed in autosomal dominant AD (ADAD) or Down syndrome (DS) (Scheuner et al., 1996). From a large body of data, it is clear that overproduction or altered enzymatic processing of APP are associated with a high risk of AD in ADAD and DS and the appearance of clinical AD at an earlier age (Head et al., 2016; Price and Sisodia, 1998).

Aβ positron emission tomography (PET) studies in ADAD and DS have identified a distinct pattern of early striatal deposition not commonly seen in late-onset AD (Handen et al., 2012; Klunk et al., 2007), which was confirmed in an autopsy study of ADAD

* Corresponding author at: University of Pittsburgh, 3501 Forbes Avenue, Suite 830, Room 849, Pittsburgh, PA 15213, USA. Tel.: +1 412 246.6251; fax: +1 412 264 6466.
E-mail address: cohenad@upmc.edu (A.D. Cohen).

0197-4580/$ – see front matter © 2018 Elsevier Inc. All rights reserved.
https://doi.org/10.1016/j.neurobiolaging.2018.09.030

(Shinohara et al., 2014) and DS (Braak and Braak, 1990; Mann and Iwatsubo, 1996). Although significant Aβ deposition is observed in an age- and APOEe4-dependent fashion in some nondemented elderly (NDE), a similar pattern of early striatal Aβ is not observed in the NDE (Aizenstein et al., 2008) and, in fact, it has been recently suggested that Aβ deposition in the neocortex precedes that of the striatum in the NDE (Hanseeuw et al., 2016). We have previously demonstrated significant differences in striatal Pittsburgh Compound B (PiB) retention between NDE and nondemented DS subjects (Cohen et al., 2018), and these data would suggest differences in rates of striatal and neocortical Aβ deposition between nondemented DS and NDE; there are no longitudinal data to directly support this hypothesis.

Therefore, we evaluated the longitudinal rates in early Aβ deposition in a nondemented DS population when compared to rates in an NDE population. We compared the regional trajectories over time for 3 regions: (1) anterior ventral striatum (AVS), (2) frontal cortex (FRC), and (3) precuneus (PRC), chosen a priori based on areas of known early Aβ deposition from previous studies of DS and NDE (Aizenstein et al., 2008; Handen et al., 2012; Hanseeuw et al., 2016). It was hypothesized that a DS population would differ significantly from an NDE population in terms trajectory rates of Aβ deposition in the AVS and neocortical brain regions.

2. Methods

2.1. Subjects

2.1.1. DS cohort

A total of 83 adults with confirmed DS were recruited from 2 sites, University of Wisconsin-Madison and University of Pittsburgh, as previously described (Lao et al., 2016). Briefly, exclusion criteria included having a prior diagnosis of dementia, conditions that might contraindicate magnetic resonance imaging (MRI) (e.g., claustrophobia, metal in the body), and having a medical or psychiatric condition that impaired cognitive functioning. Participants were assessed for dementia using the Down syndrome Dementia Scale (Gedye, 1995). Three individuals who received a cognitive cutoff score >3 (indicating dementia) were removed from this analysis. One individual had a cognitive cutoff score of 3 at entry but was included based on low early and middle tally score on the Down syndrome Dementia Scale, suggesting dementia was not present. Thus, 80 subjects underwent the image processing described in Section 2.2.1. All study procedures were approved by the University of Pittsburgh and the University of Wisconsin-Madison institutional review boards.

2.1.2. NDE cohort

Ninety-eight individuals recruited from the University of Pittsburgh for a longitudinal study of cognitively normal adults (NAs) were included in this work. Inclusion criteria were normal cognition and age 65 years or older. Normal cognition was classified according to consensus cognitive diagnosis, which closely follows the approach and structure of Alzheimer's Disease Research center Consensus Conference (Lopez et al., 2000). Exclusion criteria included contraindications for neuroimaging, and history of neurologic, psychiatric, or other medical conditions or treatment associated with potentially significant cognitive symptoms. All participants provided written informed consent, and all study procedures were approved by the institutional review board of the University of Pittsburgh.

2.2. Image acquisition

2.2.1. DS study

2.2.1.1. PET scans. Approximately 15 mCi of [^{11}C]PiB was delivered intravenously as a slow bolus injection (over 20–30 seconds) in the antecubital vein. [^{11}C]PiB PET data were acquired on Siemens ECAT HR+ PET scanners at both sites. A ^{68}Ge/^{68} Ga transmission scan was acquired for 6–10 min to correct for photon attenuation, followed by a 20-minute emission scan (4 × 5-minute frames) beginning 50 minutes after injection. Standard data corrections were applied including those for detector dead time, scanner normalization, scatter, and radioactive decay. Dynamic PET data were reconstructed using a filtered back-projection algorithm (Direct Inverse Fourier Transform) into a 128 × 128 × 63 matrix with voxel sizes of 2.06 × 2.06 × 2.43 mm^3. Images were filtered with a 3 mm Hann window.

2.2.1.2. MRI scans. T1-weighted MRIs were acquired on a 3T GE SIGNA 750 at the University of Wisconsin-Madison site and on a 3T Siemens Magnetom Trio at the University of Pittsburgh site. The SIGNA 750 acquisition used high-resolution volumetric spoiled gradient sequence (TI/TE/TR = 450/3.2/8.2 ms, flip angle = 12°, slice thickness = 1 mm no gap, matrix size = 256 × 256 × 156), while the Magnetom Trio acquisition used a magnetization prepared rapid acquisition gradient echo sequence (TI/TE/TR = 900/2.98/2300 ms, flip angle = 9°, slice thickness = 1.2 mm, matrix size = 160 × 240 × 256).

2.2.2. NDE study

2.2.2.1. PET scans. [^{11}C]PiB scans were acquired at the University of Pittsburgh on a Siemens ECAT HR+ scanner as described previously.

2.2.2.2. MRI scans. MRI data were collected at the University of Pittsburgh on a 3T Siemens Magnetom Trio scanner as described previously.

2.3. Image processing

MRI and [^{11}C]PiB PET images were processed as previously described (Cohen, 2009, Rosario, 2011). Dynamic PET images were visually assessed for frame-to-frame motion by generating a whole brain contour on a midtime point frame in ROI Tool software (CTI PET Systems Knoxville, TN, USA) and inspecting this contour across all other frames. If interframe motion was observed, a set of stable frames was averaged and used as reference for frame-to-frame registration as previously described (Price et al., 2005). PET data were then averaged over 50–70 minutes after injection. MRI images were manually skull-stripped and reoriented so that axial image planes were parallel to the anterior-posterior commissure line. [^{11}C]PiB images were registered to skull-stripped MRIs using rigid body registration in AIR version 3.0, and MRIs were resliced to PET resolution.

Manual region of interest (ROI) drawing was performed on skull-stripped MRIs in PET resolution using ROI Tool software (Siemens Medical Systems, Knoxville, TN, USA). ROIs drawn included the AVS, FRC, PRC, and cerebellar gray matter (CER). Standardized uptake value ratios (SUVR) were calculated for the AVS, FRC, and PRC using CER as reference.

2.4. Statistical methods

Descriptive statistics such as mean and standard deviation are presented for age and frequency percentages for sex and APOEe4 allele status (Table 1). In addition, means and standard deviations were computed for each cohort and time assessment for the continuous outcomes (AVS, FRC, and PRC) (Table 2). It is important to note that the decreasing number of participants over time is not due to attrition but rather the continuing enrollment of new participants in both studies, creating more participants with the baseline and time 2 data, than participants with data at later time

Table1
Demographic information for each cohort

Measure	Category	Down syndrome (N = 80)	Normal aging (N = 98)	Test statistic, *p*-value
		Mean (SD) or N (%)	Mean (SD) or N (%)	
Age at baseline		37.2 (6.9)	73.5 (5.6)	T(176) = −38.88, $p < 0.0001$
Sex	Female	38 (47.5%)	65 (66.3%)	X(1) = 6.40,
	Male	42 (52.5%)	33 (33.7%)	$p = 0.011$
APOEe4	Negative	63 (78.8%)	63 (64.3%)	X(1) = 0.70,
	Positive	12 (15.0%)	17 (17.3%)	$p = 0.402$
	Missing	5 (6.3%)	18 (18.4%)	

points. In Table 2, for descriptive purposes, data are presented as 5 time points that ranged ±6 months for each of the 5 time assessments. We refer to the baseline or time 0 as first measurement, time 2 as second measurement that was assessed at 24 months ± 6, time 3 as 3rd measurement at 36 months ± 6, time 4 was 48 months ± 6, and so forth. Time was used as continuous variable in our models to account for the fact that subject measurements were not equally spaced between time assessments.

To assess the differences in the trajectories of Aβ deposition over time between the NDE and DS cohorts, for each of the 3 ROI's SUVR, a repeated measures model was used. The model was fit for each ROI separately. Best fits were determined via Wald t-tests for the fixed effects and by minimizing the Bayesian Information Criterion for determining the best fitting random effects parameters. The fixed effect parameters were included if the Wald t-tests had *p*-values ≤ 0.05. Each of the best models included a fixed factor of cohort, a fixed effect of time, age at the baseline, and a fixed interaction term between time and cohort, cohort and age, and a random intercept and slope to account for within-subject correlation. The interaction effect between time and cohort was used to explore the differences in the Aβ trajectories between the DS and NDE cohorts, and the interaction term between cohort and age was used to explore the differences between the 2 groups with respect to age. The Kenward-Roger method (Kenward and Roger, 1997) was used for computing the degrees of freedom. The following statistical model was fit for each ROI SUVR (y):

$$y_{ij} = \beta_0 + \beta_1 Cohort_i + \beta_2 Time_{ij} + \beta_3 Time_{ij} \times Cohort_i + \beta_4 Age_i + \beta_5 Age_i \times Cohort_i + v_{0i} + v_{1i} Time_{ij} + \varepsilon_{ij},$$

where:

(1) β_0 represents the intercept (average SUVR value for the reference group [NA] at the baseline);
(2) $Cohort_i$ is the dummy variable for the cohort factor for subject *i* $Cohort_i = 1$ if cohort is DS, 0 if NA;
(3) $Time_{ij}$ represents the effect of time, fitted as continuous;
(4) Age_i represents age for subject *i* at the baseline; v. v_{0i} is the subject-specific variation from average intercept effect, and v_{1i} is the subject-specific variation from the average slope with the following variance/covariance matrix: $\begin{bmatrix} v_{0i} \\ v_{1i} \end{bmatrix} = N\left\{ \begin{bmatrix} 0 \\ 0 \end{bmatrix}, \begin{bmatrix} \sigma^2_{v_0} & \sigma_{v_0 v_1} \\ \sigma_{v_0 v_1} & \sigma^2_{v_1} \end{bmatrix} \right\}$ and $\varepsilon_{ij} \sim N(0, \sigma^2_e)$ is the random error term at the *j*th time point for subject *i*.

The term β_3 represents the difference in the trajectories over time between DS and NDE cohorts, the term β_5 represents the age difference between the cohorts and the β_2 and β_1 represent the estimates of main effects of cohort and time.

3. Results

Mean ages at the baseline were 37.2 for the DS (minimum age was 30 years and maximum was 53 years) and 73.5 for the NDE (minimum age of 65 years and maximum of 88 years) cohorts, respectively (Table 1). There were significant differences in terms of age between the 2 cohorts (Table 1, $p < 0.0001$). The DS cohort had a nearly equal proportion of males and females, whereas the NDE cohort had more female subjects. There were significant differences with respect to the proportion of males and females between the 2 cohorts (Table 1, $p = 0.006$); however, when we tested the addition of the variable sex in the model, it was not significant. There was a comparable incidence of APOEe4 positivity between the DS (12/75 subjects, or 16%) and NDE cohorts (17/80 subjects, or 22%) for whom data on APOEe4 status was available (Table 1). There were no statistically significant differences with respect to APOEe4 between the cohorts.

The baseline SUVR AVS value (starting point) was computed by substituting the parameters from Table 3 into the statistical model equation above. For an average-age NDE subject (73.5 years), the baseline SUVR AVS is 1.328 (0.813 + 0.007*73.5), whereas the baseline SUVR AVS for an average age DS subject (37.2 years) is equal to 1.450 (0.813−1.038+0.007 × 37.2 + 0.038 × 37.2).

The slope for the NDE AVS (the parameter corresponding to the time effect from Table 3) is 0.025 SUVR units, whereas for DS, the slope of the AVS is the sum of the parameters corresponding to the time and time x cohort interaction, 0.050 SUVR units (0.025 + 0.025). The interaction effect between time and cohort was statistically significant (F (1,120) = 7.02, $p = 0.009$), Table 3, suggesting that trajectory rates over time are different between the 2 groups (the DS has a steeper slope equal to 0.050 SUVRs, compared to 0.025 SUVRs for the NDE cohort), suggesting faster striatal Aβ deposition over time as compared to the NDE population. Similarly, the interaction effect between age and cohort was also statistically significant (F (1,176) = 21.39, $p < 0.0001$), Table 3, suggesting that

Table 2
Descriptive statistics for each ROI by cohort for each time point

	Baseline		Time 2		Time 3		Time 4		Time 5	
	n	Mean (SD)	n	Mean (SD)	n	Mean (SD)	n	Mean (SD)	n	Mean (SD)
Normal aging										
AVS	98	1.34 (0.29)	71	1.39 (0.31)	17	1.36 (0.35)	32	1.46 (0.37)	12	1.50 (0.40)
FRC	98	1.39 (0.32)	71	1.48 (0.35)	17	1.50 (0.42)	32	1.58 (0.41)	12	1.58 (0.44)
PRC	98	1.41 (0.35)	71	1.51 (0.39)	17	1.61 (0.54)	32	1.60 (0.42)	12	1.62 (0.44)
Down syndrome										
AVS	80	1.45 (0.50)	14	1.42 (0.58)	31	1.60 (0.62)	10	1.54 (0.33)	14	1.68 (0.74)
FRC	80	1.26 (0.27)	14	1.28 (0.38)	31	1.31 (0.33)	10	1.23 (0.16)	14	1.43 (0.58)
PRC	80	1.37 (0.30)	14	1.40 (0.44)	31	1.42 (0.35)	10	1.37 (0.19)	14	1.52 (0.54)

Data is presented as mean (standard deviation).
Key: ROI, region of interest; SD, standard deviation.

Table 3
Repeated measures analysis estimates adjusted for age at entry

Effect	β (SE)	t (DF)	*p*-value	95% CI for β
AVS				
Intercept	0.813 (0.448)	1.801(175)	<0.0001	(−0.071, 1.697)
Cohort	−1.037 (0.494)	−2.10 (175)	0.037	(−2.013, −0.062)
Time	0.025 (0.006)	4.09 (112)	<0.0001	(0.013, 0.038)
Time × Cohort	0.025 (0.009)	2.63 (120)	0.009	(0.006, 0.044)
Age	0.007 (0.006)	1.18 (175)	0.238	(−0.004, 0.019)
Age × Cohort	0.040 (0.008)	4.62 (176)	<0.0001	(0.022, 0.054)
FRC				
Intercept	0.746 (0.366)	2.04 (178)	0.043	(0.023, 1.470)
Cohort	−0.330 (0.404)	−0.82 (179)	0.416	(−1.127, 0.468)
Time	0.046 (0.006)	8.21 (112)	<0.0001	(0.035, 0.057)
Time × Cohort	−0.020 (0.008)	−2.29 (120)	0.024	(−0.037, −0.003)
Age	0.009 (0.005)	1.74 (178)	0.083	(−0.001, 0.018)
Age × Cohort	0.014 (0.007)	2.06 (180)	0.040	(0.001, 0.027)
PRC				
Intercept	0.782 (0.406)	1.92 (177)	0.057	(−0.020, 1.584)
Cohort	−0.322 (0.446)	−0.72 (178)	0.507	(−1.82, 0.587)
Time	0.049 (0.006)	8.44 (117)	<0.0001	(0.037, 0.060)
Time × Cohort	−0.018 (0.006)	−2.05 (125)	0.049	(−0.035, −0.0002)
Age	0.009 (0.006)	1.56 (177)	0.123	(−0.002, 0.019)
Age × Cohort	0.016 (0.007)	2.17 (178)	0.043	(0.0004, 0.030)

Key: FRC, frontal cortex; PRC, precuneus.

the relationship between striatal Aβ deposition and age is different between the DS and NDE cohorts.

The FRC SUVR trajectories are distinct from what we observed for the AVS SUVR, starting with a higher intercept value for the FRC SUVR baseline measurement for the NDE, equal to 1.41 and a lower 1 for the DS, 1.27, computed as described previously for the AVS ROI. The slope for the NDE FRC was 0.046 SUVR units, whereas for the DS FRC was 0.026 SUVR units. For this particular brain area, NDE demonstrated faster accumulation rates over time compared to DS. The interaction effect between cohort and time was statistically significant, ($F(1, 120) = 5.23$, $p = 0.024$) suggesting that FRC Aβ deposition rates are different between the DS versus the NDE cohorts, with the NDE cohort having faster Aβ deposition over time in the FRC area as compared to DS. Similarly, the interaction effect between age and cohort was also statistically significant ($F(1,180) = 4.25$, $p = 0.040$) suggesting that the relationship between PRC Aβ deposition and age is different between the DS and NDE. The PRC area of the brain behaved in a very similar matter as the FRC (Table 3).

Fig. 1A–C present spaghetti plots of individual trajectories of Aβ deposition values over time for AVS (Fig. 1A), FRC (Fig. 1B), and PRC (Fig. 1C).

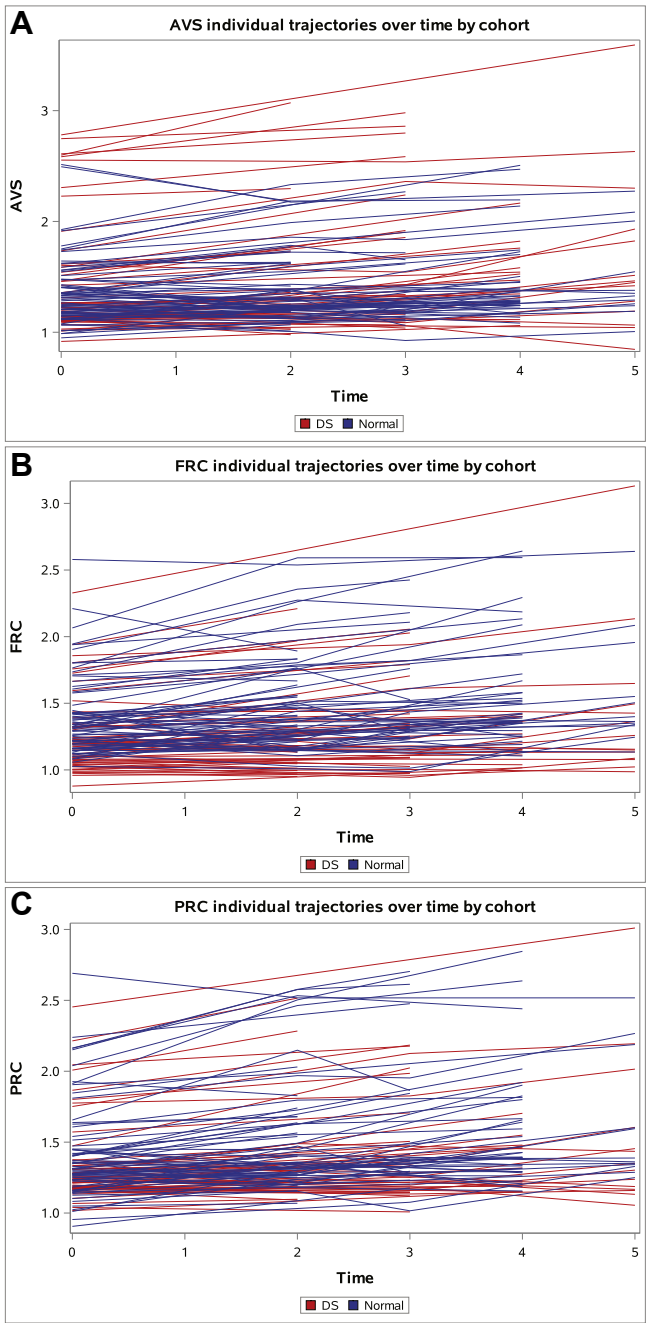

Fig. 1. Individual trajectories of change in amyloid over time by region, red denotes NDE and blue denotes DS. (A) Striatum, (B) frontal cortex, and (C) precuneus. Abbreviations: NDE, nondemented elderly; DS, Down syndrome; PRC, precuneus; AVS, anterior ventral striatum. (For interpretation of the references to color in this figure legend, the reader is referred to the Web version of this article.)

4. Discussion

Consistent with our hypothesis, we demonstrated that there were significant differences between DS and NDE cohort Aβ deposition trajectories in the striatum and neocortex. DS and NDE participants differed significantly in longitudinal change in [^{11}C]PiB in both AVS and neocortical ROIs, with faster accumulation of Aβ in DS relative to NDE in AVS and slower accumulation in neocortical regions. This work extends the findings of disproportionately high, early striatal Aβ deposition in DS relative to NDE by exploring the pattern of longitudinal change in Aβ deposition in DS and NDE. These data further highlight the unique characteristic of Aβ deposition that appears to be related to a life-long alteration of the dynamics of APP production and/or processing in DS (Cohen et al., 2018; Handen et al., 2012; Lao et al., 2016, 2017). Unlike the nonspecific retention of many tau-PET ligands in the striatum (Pontecorvo et al., 2017) and the nonspecific retention of amyloid-PET ligands in white matter (Rowe et al., 2010; Villemagne et al., 2012), the retention of PiB in the striatum specifically represents Aβ deposition (Klunk et al., 2007) that differs from NDE subjects with significant Aβ deposition (Cohen et al., 2018). Although early striatal predominance in DS has now been well established, to our knowledge, this is the first study to demonstrate differences in the longitudinal trajectory of [^{11}C]PiB retention (i.e., Aβ deposition) between individuals with DS and NDE.

The mechanism behind the phenomenon of increased striatal Aβ deposition and accumulation in DS is not well understood. Pathological studies demonstrated increased Aβ-42 relative to Aβ-40 and increased diffuse subcortical plaques in DS compared to late-onset

AD (Fukuoka et al., 1990; Kida et al., 1995; Shinohara et al., 2014). In addition, it has been demonstrated that Aβ-42 plaques are the first to develop (Lemere et al., 1996). The phenomenon of increased Aβ-42 plaques has also been demonstrated in ADAD, which like DS is associated with overproduction of Aβ and early striatal Aβ predominance (Klunk et al., 2007; Potter et al., 2013). It has been suggested that perhaps the anatomical and Aβ-42 differences observed between genetic disorders associated with overproduction of Aβ (ADAD and DS), and disorders of Aβ clearance (late-onset AD) might be due to different processes contributing to plaque development in each disorder (13). In this scenario, late-onset AD is associated more with an increased dependence of APP processing on synaptic activity, thereby increasing the cortical deposition. In ADAD or DS, increased Aβ-42 levels might relate to alterations in APP metabolism that result in early increases in APP products. This increased production then eventually overwhelms mechanisms for Aβ clearance (Shinohara et al., 2014). It may be that the production/clearance ratios in DS and ADAD are highest in the striatum.

An important consideration in the present study was difference in age between the 2 groups. The differences in mean age between the 2 groups are a consequence of the biological question being explored, that is, are there early differences in Aβ accumulation over time between a population known to overproduce Aβ (DS) and 1 that is believed to have reduced Aβ clearance (NDE). As age is one of the most significant risk factors for Aβ deposition, in both DS (Lao et al., 2016) and normal aging (Jack et al., 2017; Rowe et al., 2010), it was important to consider the relative impact of age on longitudinal change of Aβ. Interestingly, we found a significant cohort × age interaction in each of the regions explored, suggesting that in DS, aging produces a greater relative increase of Aβ in the striatum than in the NDE, with the opposite being true in the cortical regions explored (Table 3).

Another consideration in the present study is the use of the cerebellum as a reference region. We acknowledge the findings reported in the literature of improved sensitivity using the white matter reference region within the context of longitudinal studies(Brendel et al., 2015; Chen et al., 2015; Schwarz et al., 2017), particularly related to addressing the shortcomings of technical variability introduced by differences in scanner slice sensitivity and noise. However, we feel strongly that CER reference region provides a more accurate physiological representation of amyloid burden. Considering the SUVR metric serves as a proxy for the distribution volume ratio or binding potential, the nondisplaceable distribution volume (V_ND = K1/k2′) should be close to equal in these gray matter tissue regions (and thus cancel out in the ratio), and that the overall findings would be expected to be compatible.

A limitation of the present study was the variation in follow-up time between the DS cohort and the NDE cohort. To address the differences in follow-up time between the 2 cohorts, we treated time as a continuous variable in the models to explore the relationship between group and time. However, as can be seen in Table 2, for descriptive purposes, we presented the data as 5 time points that ranged ±6 months for each of the 5 time points. For instance, the baseline (or time 0 as presented in the plots) represents the first measurement and time 2 represents the second measurement, which was at 24 months ± 6, time 3 was 36 months ± 6, time 4 was 48 months ± 6, and so forth. In addition, another limitation of the present study is the small number of participants, particularly in the DS group at the later time points (Table 2). Because of these small group sizes, we are not powered to investigate the effect of APOEe4 on accumulation of Aβ over time.

An important question related to the differences in striatal Aβ predominance in DS (and ADAD) is if this phenomenon has any clinical or therapeutic implications. Currently, there are no clear clinical manifestations related to striatal Aβ deposition (e.g., extrapyramidal symptoms); however, a significant association between the striatal [^{11}C]PiB retention and executive cognitive function has been demonstrated in ADAD (McDade et al., 2014). It remains to be seen if similar relationships will be detected in DS—although this will be difficult to disentangle from the highly correlated increases in Aβ deposition across all affected brain areas.

What is most striking is the apparent resistance of striatal neurons to very high levels of local Aβ deposition based on the lack of significant striatal atrophy, hypometabolism, or striatal-related behavioral or motor dysfunction in either DS or ADAD. Understanding this cellular resilience could lead to novel therapeutic strategies directed at the protection of neocortical and limbic neurons. Another important consideration is whether the uniquely early striatal Aβ predominance could be used as an early marker in AD treatment trials targeting Aβ in nondemented DS in the future.

Disclosure statement

The authors report no conflicts of interest.

Acknowledgements

Supported by The National Institutes of Health grants: P50 AG005133, RF1 AG025516, R01AG031110, U01AG051406.

Authors' contributions: D.L.T., A.D.C., S.H., P.L., B.T.C., B.L.H., and W.E.K. contributed to study design. D.L.T., S.J.A., and A.D.C. contributed to article preparation. D.L.T., S.J.A., and D.C. contributed to statistical analysis. B.T.C., A.D.C., W.E.K., C.A.M., J.C.P., H.J.A., B.J.L., C.M.L., D.S.M., and B.E.S. contributed to article review/revisions. B.T.C., B.L.H., W.E.K., S.J., and H.J.A. contributed to data acquisition.

Appendix A. Supplementary data

Supplementary data associated with this article can be found, in the online version, at https://doi.org/10.1016/j.neurobiolaging.2018.09.030.

References

Aizenstein, H.J., Nebes, R.D., Saxton, J.A., Price, J.C., Mathis, C.A., Tsopelas, N.D., Ziolko, S.K., Snitz, B.E., Houck, P.R., Bi, W., Cohen, A.D., Lopresti, B.J., DeKosky, S.T., Halligan, E.M., Klunk, W.E., 2008. Amyloid deposition is frequent and often is not associated with significant cognitive impairment in the elderly. Arch. Neurol. 65, 1509–1517.

Braak, H., Braak, E., 1990. Alzheimer's disease: striatal amyloid deposits and neurofibrillary changes. J. Neuropathol. Exp. Neurol. 49, 215–224.

Brendel, M., Hogenauer, M., Delker, A., Sauerbeck, J., Bartenstein, P., Seibyl, J., Rominger, A., Alzheimer's Disease Neuroimaging I., 2015. Improved longitudinal [(18)F]-AV45 amyloid PET by white matter reference and VOI-based partial volume effect correction. Neuroimage 108, 450–459.

Chen, K., Roontiva, A., Thiyyagura, P., Lee, W., Liu, X., Ayutyanont, N., Protas, H., Luo, J.L., Bauer, R., Reschke, C., Bandy, D., Koeppe, R.A., Fleisher, A.S., Caselli, R.J., Landau, S., Jagust, W.J., Weiner, M.W., Reiman, E.M., Alzheimer's Disease Neuroimaging I., 2015. Improved power for characterizing longitudinal amyloid-beta PET changes and evaluating amyloid-modifying treatments with a cerebral white matter reference region. J. Nucl. Med. 56, 560–566.

Cohen, A.D., Price, J.C., Weissfeld, L.A., James, J., Nebes, R.D., Saxton, J.A., Snitz, B.E., Aizenstein, H.A., Wolk, D.A., DeKosky, S.T., Mathis, C.A., Klunk, W.E., 2009. Basal Cerebral Metabolism May Modulate the Cognitive Effects of Aβ in Mild Cognitive Impairment: An Example of Brain Reserve. J. Neurosci. 29, 14770–14778.

Cohen, A.D., McDade, E., Christian, B., Price, J., Mathis, C., Klunk, W., Handen, B.L., 2018. Early striatal amyloid deposition distinguishes Down syndrome and autosomal dominant Alzheimer's disease from late-onset amyloid deposition. Alzheimers Dement. 14, 743–750.

Fukuoka, Y., Fujita T., Ito H., 1990. Histopathological studies on senile plaques in brains of patients with Down's syndrome. Kobe J. Med. Sci. 36, 153–171.

Gedye, A., 1995. Dementia Scale for Down Syndrome. Gedye Research & Consulting, Vancouver, BC, Canada.

Handen, B.L., Cohen, A.D., Channamalappa, U., Bulova, P., Cannon, S.A., Cohen, W.I., Mathis, C.A., Price, J.C., Klunk, W.E., 2012. Imaging brain amyloid in

nondemented young adults with Down syndrome using Pittsburgh compound B. Alzheimers Dement. 8, 496–501.
Hanseeuw, B.J., Mormino, E.C., Schultz, A.P., Chhatwal, J.P., Rentz, D.M., Betensky, R.A., Sperling, R.A., Johnson, K., 2016. Pet staging of amyloidosis: evidence that amyloid occurs first in neocortex and later in striatum. Alzheimers Dement. 12, P20–P21.
Head, E., Lott, I.T., Wilcock, D.M., Lemere, C.A., 2016. Aging in Down syndrome and the development of Alzheimer's disease neuropathology. Curr. Alzheimer Res. 13, 18–29.
Hyman, B.T., Phelps, C.H., Beach, T.G., Bigio, E.H., Cairns, N.J., Carrillo, M.C., Dickson, D.W., Duyckaerts, C., Frosch, M.P., Masliah, E., Mirra, S.S., Nelson, P.T., Schneider, J.A., Thal, D.R., Thies, B., Trojanowski, J.Q., Vinters, H.V., Montine, T.J., 2012. National Institute on Aging-Alzheimer's Association guidelines for the neuropathologic assessment of Alzheimer's disease. Alzheimers Dement. 8, 1–13.
Jack Jr., C.R., Wiste, H.J., Weigand, S.D., Therneau, T.M., Knopman, D.S., Lowe, V., Vemuri, P., Mielke, M.M., Roberts, R.O., Machulda, M.M., Senjem, M.L., Gunter, J.L., Rocca, W.A., Petersen, R.C., 2017. Age-specific and sex-specific prevalence of cerebral beta-amyloidosis, tauopathy, and neurodegeneration in cognitively unimpaired individuals aged 50-95 years: a cross-sectional study. Lancet Neurol. 16, 435–444.
Kenward, M.G., Roger, J.H., 1997. Small sample inference for fixed effects from restricted maximum likelihood. Biometrics 53, 983–997.
Kida, E., Wisniewski, K.E., Wisniewski, H.M., 1995. Early amyloid-beta deposits show different immunoreactivity to the amino- and carboxy-terminal regions of beta-peptide in Alzheimer's disease and Down's syndrome brain. Neurosci. Lett. 193, 105–108.
Klunk, W.E., Price, J.C., Mathis, C.A., Tsopelas, N.D., Lopresti, B.J., Ziolko, S.K., Bi, W., Hoge, J.A., Cohen, A.D., Ikonomovic, M.D., Saxton, J.A., Snitz, B.E., Pollen, D.A., Moonis, M., Lippa, C.F., Swearer, J.M., Johnson, K.A., Rentz, D.M., Fischman, A.J., Aizenstein, H.J., DeKosky, S.T., 2007. Amyloid deposition begins in the striatum of presenilin-1 mutation carriers from two unrelated pedigrees. J. Neurosci. 27, 6174–6184.
Lao, P.J., Betthauser, T.J., Hillmer, A.T., Price, J.C., Klunk, W.E., Mihaila, I., Higgins, A.T., Bulova, P.D., Hartley, S.L., Hardison, R., Tumuluru, R.V., Murali, D., Mathis, C.A., Cohen, A.D., Barnhart, T.E., Devenny, D.A., Mailick, M.R., Johnson, S.C., Handen, B.L., Christian, B.T., 2016. The effects of normal aging on amyloid-beta deposition in nondemented adults with down syndrome as imaged by carbon 11-labeled Pittsburgh compound B. Alzheimers Dement. 12, 380–390.
Lao, P.J., Handen, B.L., Betthauser, T.J., Mihaila, I., Hartley, S.L., Cohen, A.D., Tudorascu, D.L., Bulova, P.D., Lopresti, B.J., Tumuluru, R.V., Murali, D., Mathis, C.A., Barnhart, T.E., Stone, C.K., Price, J.C., Devenny, D.A., Mailick, M.R., Klunk, W.E., Johnson, S.C., Christian, B.T., 2017. Longitudinal changes in amyloid positron emission tomography and volumetric magnetic resonance imaging in the non-demented down syndrome population. Alzheimers Dement. (Amst). 9, 1–9.
Lemere, C.A., Blusztajn, J.K., Yamaguchi, H., Wisniewski, T., Saido, T.C., Selkoe, D.J., 1996. Sequence of deposition of heterogeneous amyloid β^2-peptides and APO E in Down syndrome: implications for initial events in amyloid plaque formation. Neurobiol. Dis. 3, 16–32.
Lopez, O.L., Becker, J.T., Klunk, W.E., Saxton, J., Hamilton, R.L., Kaufer, D.I., Sweet, R.A., Cidis-Meltzer, C., Wisniewski, S., Kamboh, M.I., DeKosky, S.T., 2000. Research evaluation and diagnosis of probable Alzheimer's disease over the last two decades. Neurology 55, 1854–1862.
Mann, D.M., Iwatsubo, T., 1996. Diffuse plaques in the cerebellum and corpus striatum in Down's syndrome contain amyloid beta protein (A beta) only in the form of A beta 42(43). Neurodegeneration 5, 115–120.
Mawuenyega, K.G., Sigurdson, W., Ovod, V., Munsell, L., Kasten, T., Morris, J.C., Yarasheski, K.E., Bateman, R.J., 2010. Decreased clearance of CNS beta-amyloid in Alzheimer's disease. Science 330, 1774.
McDade, E., Kim, A., James, J., Sheu, L.K., Kuan, D.C., Minhas, D., Gianaros, P.J., Ikonomovic, S., Lopez, O., Snitz, B., Price, J., Becker, J., Mathis, C., Klunk, W., 2014. Cerebral perfusion alterations and cerebral amyloid in autosomal dominant Alzheimer disease. Neurology 83, 710–717.
Pontecorvo, M.J., Devous Sr, M.D., Navitsky, M., Lu, M., Salloway, S., Schaerf, F.W., Jennings, D., Arora, A.K., McGeehan, A., Lim, N.C., Xiong, H., Joshi, A.D., Siderowf, A., Mintun, M.A., 18F-AV-1451-A05 Investigators, 2017. Relationships between flortaucipir PET tau binding and amyloid burden, clinical diagnosis, age and cognition. Brain 140, 748–763.
Potter, R., Patterson, B.W., Elbert, D.L., Ovod, V., Kasten, T., Sigurdson, W., Mawuenyega, K., Blazey, T., Goate, A., Chott, R., Yarasheski, K.E., Holtzman, D.M., Morris, J.C., Benzinger, T.L.S., Bateman, R.J., 2013. Increased in vivo amyloid-beta 42 production, exchange, and loss in presenilin mutation carriers. Sci. Transl. Med. 5, 189ra77.
Price, D.L., Sisodia, S.S., 1998. Mutant genes in familial Alzheimer's disease and transgenic models. Annu. Rev. Neurosci. 21, 479–505.
Price, J.C., Klunk, W.E., Lopresti, B.J., Lu, X., Hoge, J.A., Ziolko, S.K., Holt, D.P., Meltzer, C.C., Dekosky, S.T., Mathis, C.A., 2005. Kinetic modeling of amyloid binding in humans using PET imaging and Pittsburgh Compound-B. J. Cereb. Blood Flow Metab. 25, 1528–1547.
Rosario, B.L., Weissfeld, L.A., Laymon, C.M., Mathis, C.A., Klunk, W.E., Berginc, M.D., James, J.A., Hoge, J.A., Price, J.C., 2011. Inter-rater reliability of manual and automated region-of-interest delineation for PiB PET. Neuroimage 55, 933–941.
Rowe, C.C., Ellis, K.A., Rimajova, M., Bourgeat, P., Pike, K.E., Jones, G., Fripp, J., Tochon-Danguy, H., Morandeau, L., O'Keefe, G., Price, R., Raniga, P., Robins, P., Acosta, O., Lenzo, N., Szoeke, C., Salvado, O., Head, R., Martins, R., Masters, C.L., Ames, D., Villemagne, V.L., 2010. Amyloid imaging results from the Australian imaging, biomarkers and lifestyle (AIBL) study of aging. Neurobiol. Aging 31, 1275–1283.
Scheuner, D., Eckman, C., Jensen, M., Song, X., Citron, M., Suzuki, N., Bird, T.D., Hardy, J., Hutton, M., Kukull, W., Larson, E., Levy-Lahad, E., Viitanen, M., Peskind, E., Poorkaj, P., Schellenberg, G., Tanzi, R., Wasco, W., Lannfelt, L., Selkoe, D., Younkin, S., 1996. Secreted amyloid beta-protein similar to that in the senile plaques of Alzheimer's disease is increased in vivo by the presenilin 1 and 2 and APP mutations linked to familial Alzheimer's disease. Nat. Med. 2, 864–870.
Schwarz, C.G., Senjem, M.L., Gunter, J.L., Tosakulwong, N., Weigand, S.D., Kemp, B.J., Spychalla, A.J., Vemuri, P., Petersen, R.C., Lowe, V.J., Jack Jr, C.R., 2017. Optimizing PiB-PET SUVR change-over-time measurement by a large-scale analysis of longitudinal reliability, plausibility, separability, and correlation with MMSE. Neuroimage 144, 113–127.
Shinohara, M., Fujioka, S., Murray, M.E., Wojtas, A., Baker, M., Rovelet-Lecrux, A., Rademakers, R., Das, P., Parisi, J.E., Graff-Radford, N.R., Petersen, R.C., Dickson, D.W., Bu, G., 2014. Regional distribution of synaptic markers and APP correlate with distinct clinicopathological features in sporadic and familial Alzheimer's disease. Brain 137, 1533–1549.
Villemagne, V.L., Mulligan, R.S., Pejoska, S., Ong, K., Jones, G., O'Keefe, G., Chan, J.G., Young, K., Tochon-Danguy, H., Masters, C.L., Rowe, C.C., 2012. Comparison of 11C-PiB and 18F-florbetaben for Abeta imaging in ageing and Alzheimer's disease. Eur. J. Nucl. Med. Mol. Imaging 39, 983–989.